Modeling the Snoek peak in bct-martensite

Philippe Maugis, Liangzhao Huang

Modeling the Snoek peak in bct-martensite

Philippe Maugis, Liangzhao Huang

Aix Marseille University, CNRS, IM2NP, Marseille, France

Abstract

Snoek relaxation in bcc crystals is the delayed strain response to an applied stress resulting from the interaction of the interstitial atoms with the stress field. It is responsible for the Snoek peak observed in internal friction measurements of ferrite. However, although martensite is carbon supersaturated, several authors denied the possibility of Snoek relaxation in bct-martensite. We investigated this matter by means of Monte Carlo simulations and mean-field thermo-kinetic modeling. Our results show that Snoek relaxation does occur in bct-martensite. The computed Snoek profiles of temperature-dependent and frequency-dependent internal friction exhibit unexpected features: both peak height and peak temperature decrease when the carbon content is increased. We explain this behavior in the frame of the linear-response approximation. Our theoretical predictions are in qualitative agreement with experiments.

Keywords: anelastic behavior, internal friction, long-range ordering, carbon steels, mean-field modeling, Monte Carlo simulation

1. Introduction

The internal friction response of carbon steel depends on whether the crystal phase is ferrite or martensite: Fe-C ferrite exhibits the so-called Snoek peak at a temperature of $\sim$ 310 K for an excitation frequency of 1 Hz. The peak height is found proportional to the carbon content [1, 2]. On the other side, martensite reveals a complex landscape. Various peaks are reported in the literature, and their origin is a subject of debate [2, 3]. Around room temperature under low frequency excitation, four types of thermally activated peaks were identified: (1) $\sim$ 260 K (-10°C) [4–11], (2) $\sim$ 310 K (40°C) [12–16], (3) $\sim$ 350 K (80°C) [17–20] and (4) $\sim$ 430 K (160°C) [21–24]. Among them, the peaks of type (1) or (2) are sometimes described as Snoek or Snoek-like peaks [12–16, 21, 24].

The term "martensite" is somehow confusing in this context. Some authors define martensite as the microstructure resulting from the quench of a parent high-temperature austenite phase, whatever the crystal structure of the daughter phase (bcc or bct). We will refer to that microstructural component as "martensitic microstructure". Conversely, martensite can be defined more restrictively as the tetragonal crystal structure wherein carbon atoms occupy preferentially one type of octahedral site. We will refer to that phase as "bct-martensite". Yet, due to auto-tempering during the quench, to tempering or to aging phenomena, a martensitic microstructure may consist of a mixture of bcc-ferrite grains and transition carbides. Thus, the low levels of solute carbon in the ferrite grains of the microstructure produce a Snoek peak [12–16]. True bct-martensite is usually obtained by cryogenic quench of plain Fe-C steel with carbon content greater than $\sim$ 0.2 wt% (fresh martensite), or of alloyed Fe-Ni-C steel with sub-zero Ms temperature (virgin martensite). In these cases, the usual $\sim$ 310 K Snoek peak is not observed, but a near 260 K peak is sometimes apparent [5–11].

The origin of the Snoek peak in ferrite is well understood. The peak results from the relaxation of carbon atoms over the interstitial sublattices [25]: an applied mechanical stress creates biases in carbon chemical potential between the three sets of octahedral sites. Fluxes of carbon atoms set up between the sublattices, generating the anelastic strain. The time lag between the applied stress and the anelastic response produces a measurable energy loss. When the excitation frequency is close to the frequency of the carbon jumps, the energy loss rises and the internal friction signal peaks.

On the other hand, the possibility of a Snoek peak in bct-martensite was denied by several authors [10, 15, 22, 26, 27]. Their argument is the following: in martensite, the carbon atoms are "trapped" in the so-called favored sites of the bct lattice. Unless a very high stress is applied, the carbon atoms cannot jump out of their sites towards disfavored sites. In response to that reasoning, we put forward the following argument: actually, no carbon atom is indefinitely trapped in the structure. Indeed, migration enthalpies in martensite differ from ferrite, but they remain finite [28–30]. Consequently, an applied stress creating a bias in chemical potential will induce a net flux of carbon atoms from one set to the others, i.e. a Snoek relaxation. On account of the tetragonal symmetry of the crystal, carbon diffusion in bct-martensite is known to be anisotropic (parallel and perpendicular components differ [28–30]), so that two characteristic times are expected. For the same symmetry reason, Snoek relaxation will depend on whether the axis of the shear stress excitation is parallel or perpendicular to the axis of tetragonality. Last, since carbon ordering

in deformed bct-martensite is described by two order parameters [31, 32], two relaxation modes are expected (parallel and perpendicular modes) [25].

In this article, we report our theoretical investigation of Snoek relaxation in bct-martensite. The underlying theory based on the elasto-chemical model is presented. The thermo-kinetic model is used to compute the influence of composition, temperature and frequency on relaxation. The results are compared to atomic-scale Monte Carlo simulations. The approximate linear-response theory allows rationalizing our results. Striking features of the Snoek peak in bct-martensite are highlighted. Our findings are discussed and compared to the experimental literature. Finally, specific experimental investigations are suggested to test our predictions quantitatively.

2. The thermo-kinetic model

The thermo-kinetic model describes the thermodynamics of carbon long-range ordering together with the dynamics of carbon atomic jumps in body-centered crystals. It is based on a mean-field approximation of the long-range carbon–carbon elastic interaction. The model accounts for Zener ordering [32, 33], carbon diffusion [30] and thermo-elasticity of both bcc-ferrite and bct-martensite [31, 34]. It renders quantitatively the Snoek peak of ferrite [35, 36]. It was used in this study to compute the energy loss of a martensite variant submitted to an oscillatory shear stress. The main features of the model are described below, details can be found in Ref. [34].

2.1. Crystal geometry

Carbon atoms soluted in body-centered iron can sit on three types of octahedral lattice site, with respective molar fractions c_i ($i = 1, 2, 3$) (Figure 1, left). Above the temperature of Zener [37] order–disorder transition, bcc-ferrite is thermodynamically stable, wherein the three types of sites are equally occupied. Below the transition temperature, three orientational variants of bct-martensite are stable, labeled Z1, Z2 and Z3 according to the direction of the tetragonality axis. In variant Z3, for instance, the sites of type-3 are energetically favored by the carbon–carbon elastic interactions, such that these sites are preferentially occupied relative to disfavored sites of type-1 and 2. In each variant, favored sites are noted 'c' and disfavored sites are noted 'a'. Under a given total fraction $C = \sum c_i$, the distribution of carbon atoms over the octahedral sites is described by the long-range order parameters $\eta = \left(c_3 - \frac{1}{2}(c_1 + c_2)\right)/C$ and $\zeta = (c_2 - c_1)/C$. Parameter η quantifies the degree of Zener order along crystal direction [001], while ζ quantifies the unequal occupancy of the sites in directions [100] and [010]. In the mean-field approximation, a variant of martensite is characterized by the couple of values (ζ, η).

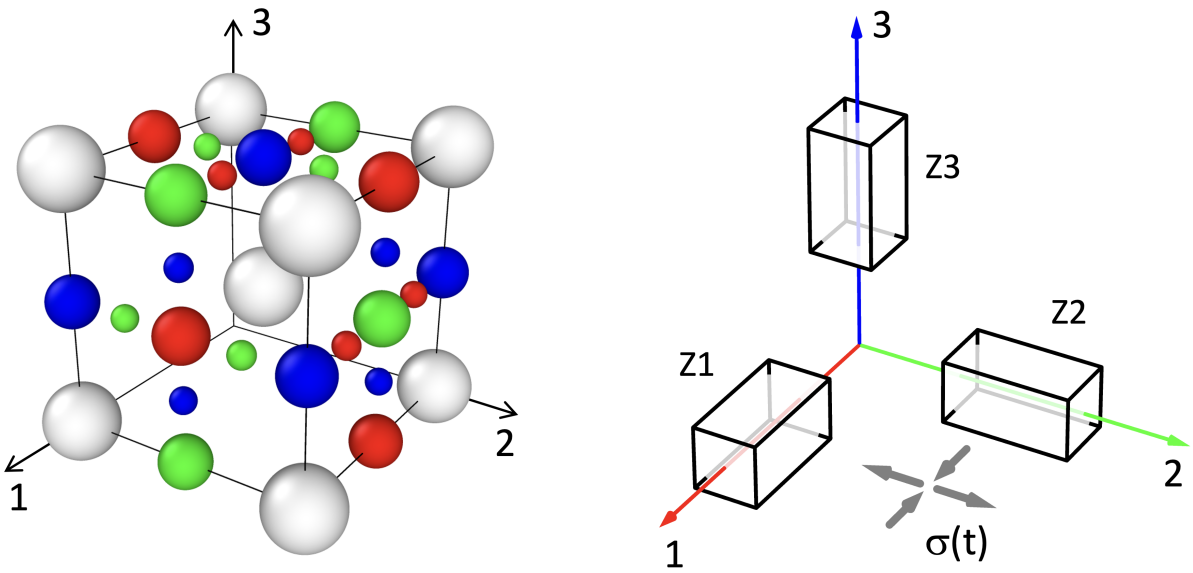

Figure 1: Left: Crystal sites in body centered iron. Iron atoms are represented by gray spheres, octahedral sites by large colored spheres and tetrahedral sites by small colored spheres. Sites of type 1, 2, 3 are respectively in color red, green, blue. Right: Under applied stress with shear axis along [001] direction (gray arrows), the excitation is transversal for variant Z3 and longitudinal for variants Z1 and Z2.

To study the elastic response of a martensite variant, we considered a crystal submitted to pure $(1\bar{1}0)[110]$ shear stress such that $\sigma_{22} = -\sigma_{11} = \sigma(t)$. The anelastic response depends on the crystal orientation relative to the stress. Given the tetragonal symmetry of martensite variants, two types of mechanical excitation were defined (Figure 1, right):

1. Transversal excitation when the shear axis is parallel to the tetragonality axis. It is the case of variant Z3;

2. Longitudinal excitation when the shear axis is perpendicular to the tetragonality axis. It is the case of variants Z1 and Z2.

2.2. Alloy thermodynamics

Carbon atoms migrate via three types of tetrahedral sites, labeled $j = 1, 2, 3$. The far-end elastic field induced by a carbon atom is characterized by the force dipole tensor of the site: $\boldsymbol{P}^{\mathrm{O}_i}$ in octahedral site or $\boldsymbol{P}^{\mathrm{T}_j}$ in tetrahedral site. In our mean-field approach, each carbon atom interacts with the elastic field created by both the applied stress and the other carbon atoms. The resulting homogeneous strain tensor $\boldsymbol{\varepsilon}$ is expressed as a function of the stress tensor $\boldsymbol{\sigma}$ and of the force dipole density tensor $\boldsymbol{p}$ as:

$$\boldsymbol{\varepsilon} = \boldsymbol{S}\,(\boldsymbol{\sigma} + \boldsymbol{p})\,, \tag{1}$$

where $\boldsymbol{S}$ is the elastic compliance tensor of the crystal. Force dipole density $\boldsymbol{p}$ depends on the distribution of the carbon atoms over the sites. If all carbon atoms lie on octahedral sites, $\boldsymbol{p}$ is written

$$\boldsymbol{p} = \frac{1}{V_0} \sum c_i \boldsymbol{P}^{\mathrm{O}_i}, \tag{2}$$

where V_0 is the atomic volume of the lattice. In stress-free martensite, the tetragonal lattice distortion is accounted for by the deviatoric part of the density tensor $\boldsymbol{p}$. When a stress $\boldsymbol{\sigma}$ is applied, the stress-induced carbon jumps modify the distribution of the carbon atoms over the sites, which reflects in a change of the density tensor (Eq. 2). This relaxation results in the anelastic strain $\boldsymbol{Sp}$ (Eq. 1). For a given distribution of the carbon atoms over the interstitial sites, the elastic contribution to the enthalpy is written, per iron atom,

$$H = -\frac{1}{2} V_0 \boldsymbol{S}(\boldsymbol{\sigma} + \boldsymbol{p}) \cdot (\boldsymbol{\sigma} + \boldsymbol{p}). \tag{3}$$

We introduce the strain dipole tensor $\boldsymbol{\lambda} = \boldsymbol{SP}/V_0$, which quantifies the tetragonal distortion induced by a carbon atom. The strain dipole tensors have a singlet component λ_1 representing the strain along the tetragonality axis, and a doublet component λ_2 representing the strain in perpendicular directions.

2.3. The rate equations

The migration enthalpy of a carbon atom jumping from site i through transition site j is written [38]

$$H^{\mathrm{m}}_{i/j} = H^{\mathrm{m}}_0 - V_0 \left(\boldsymbol{\lambda}^{T_j} - \boldsymbol{\lambda}^{O_i}\right) \cdot (\boldsymbol{\sigma} + \boldsymbol{p}), \tag{4}$$

where H^{m}_0 is the migration enthalpy in cubic low-carbon ferrite. In tetragonal martensite, the migration enthalpy splits into three independent values. For instance, in variant-3, the migration enthalpies write $H^{\mathrm{m}}_{1/2}$, $H^{\mathrm{m}}_{1/3}$ and $H^{\mathrm{m}}_{3/1}$. The jump probability for a carbon atom is written, according to the jump rate theory,

$$p_{i/j} = \nu_0 \exp\left(-H^{\mathrm{m}}_{i/j}/k_{\mathrm{B}}T\right), \tag{5}$$

where ν_0 is a constant attempt frequency. From the probability function Equation 5, the time evolution of a set of carbon atoms we can simulated by on-lattice atomic kinetic Monte Carlo (AKMC [30, 34, 35, 38]). Alternatively, a mean-field approximation can be used (thermo-kinetic model [36]). In the latter approach, the jump frequency is written

$$\Gamma_{i/j} = c_i p_{i/j}. \tag{6}$$

The net atom flux from stable position i to stable position k via saddle position j is

$$J_{i\to k} = \Gamma_{i/j} - \Gamma_{k/j}. \tag{7}$$

Matter balance at site i implies the rate equations

$$\dot{c}_i = 2\,(J_{k\to i} + J_{k'\to i})\,, \quad i = 1, 2, 3. \tag{8}$$

Integrating Equations (8) provides the time evolution of the site fractions $c_i(t)$ under given applied stress. The resulting strain response is given by Equations 1 and 2.

3. Results: internal friction profiles

The thermo-kinetic model was first benchmarked versus Monte Carlo simulations. It was then employed to compute temperature-dependent and frequency-dependent internal friction profiles for various carbon contents in bcc-ferrite and bct-martensite.

Table 1: Material parameters used for the computations: lattice parameter a_0 (in nm), elastic compliances S_{ij} (in GPa^{-1}), force dipole components P_a and P_c for octahedral (O) and tetrahedral (T) positions (in eV), migration enthalpy H_0^m (in eV) and attempt frequency ν_0 (in THz).

a_0	S_{11}	S_{12}	S_{44}	P_c^O	P_a^O	P_c^T	P_a^T	H_0^m	ν_0
0.2855	0.00615	−0.00218	0.0104	17.0	10.0	5.37	14.8	0.872	159

3.1. Model parameters and computational set up

Our computations used no fitting parameter: the material parameters were computed previously by density functional theory (DFT), except for ν_0 and H_0^m, which were extracted from the diffusion data of da Silva [39]. The values are gathered in Table 1. The corresponding components of the λ-tensor are $\lambda_1 = 0.838$ and $\lambda_2 = 0.035$. Our set of parameters offers a good agreement with the Snoek peak measured by Weller in ferrite [40] (see Ref. [36]).

Internal friction is defined as the fractional energy loss $Q^{-1} = (1/2\pi)\,\delta W/W^{el}$. W^{el} is the maximum elastically stored energy per unit volume during a cycle, i.e $W^{el} = \frac{1}{2}J_U\sigma_0^2$, where $J_U = 2(S_{11} - S_{12})$ is the unrelaxed compliance and σ_0 is the stress amplitude; δW is computed as the integral of $\boldsymbol{\sigma}\cdot\mathrm{d}\boldsymbol{\varepsilon}$ along a cycle. The relative storage compliance is defined as $J_1/J_U = W/W^{el}$ where the stored energy W is the integral of $\boldsymbol{\sigma}\cdot\mathrm{d}\boldsymbol{\varepsilon}$ along one fourth of a cycle. The stress amplitude was set to $\sigma_0 = 1$ MPa for the thermo-kinetic computations and to 100 MPa for the Monte Carlo simulations. To simulate internal friction measurements upon heating of the martensite phase, the initial state of the crystal before cycling was Zener ordered along a chosen direction.

To build the temperature–dependent internal friction profiles, the energy loss was computed at successive temperatures in the range of 250 to 450 K, at the oscillation frequency $f = 1$ Hz, for carbon contents ranging from 0.85 to 4.7 at%. Alternatively, frequency–dependent profiles were computed in the frequency range of 10^{-3} to 10^3 Hz at temperature $T = 300$ K. In martensite, both transversal and longitudinal orientations were considered. As a rough estimate, the average energy loss was defined as $Q^{-1} = \frac{1}{3}Q^{-1}_{trans} + \frac{2}{3}Q^{-1}_{longi}$.

3.2. Comparison with kinetic Monte Carlo

The kinetic Monte Carlo model was developed to investigate the thermodynamic, thermo-elastic and kinetic properties of Fe-C crystals. It is described in details in Ref. [30]. It uses the residence time algorithm to simulate thermally activated migration of carbon atoms in body-centered lattices. It modeled with success the Snoek peak in ferrite [36] and in martensite [41]. To check the accuracy of the thermo-kinetic (TK) equations in the case of martensite, we compared the results of the thermo-kinetic model with atomic kinetic Monte Carlo (AKMC) simulations. Both computations ran with the same set of material parameters (Table 1). The internal friction profiles computed for a martensite crystal of carbon content $C = 3$ at% under an oscillation frequency of $f = 1$ Hz are in agreement with one another (Figure 2). This test confirms that the thermo-kinetic model adequately describes the diffusion mechanisms at the origin of internal friction in martensite.

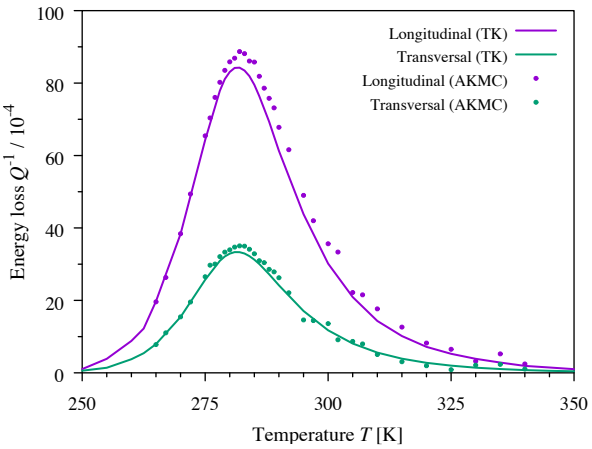

Figure 2: Comparison between the thermo-kinetic model (TK) and Monte Carlo simulations (AKMC). Snoek peaks in martensite for carbon fraction $C = 3$ at% and oscillation frequency $f = 1$ Hz. Longitudinal (violet) and transversal (green) excitations.

3.3. Temperature-dependent Snoek profiles

We computed a series of Snoek profiles upon heating in the temperature range of 250 to 450 K for various carbon contents. Previous theoretical investigations evidenced that the height, position and shape of the Snoek peak in ferrite depend on the proximity of the bcc crystal to the ferrite–martensite phase transition [35, 36]. According to the elasto-chemical model [33], the transition temperature of martensite upon heating is proportional to the carbon content

in solid solution: with our parameters, the transition temperature is numerically $T^+ = 238\,C$ (C in at%). Hence, by varying the carbon content from 0.85 to 3.7 at%, the transition temperature can be varied from 202 to 880 K. Consequently, during a temperature-dependent internal friction computation in the range of temperature 250–450 K, the crystal can be ferritic, martensitic or undergo a transition from martensite to ferrite, depending on the carbon content. To illustrate the consequences on the energy loss profiles, our computation results are gathered in Figure 3. We see that the magnitude, position and shape of the peaks depend strongly on the carbon content.

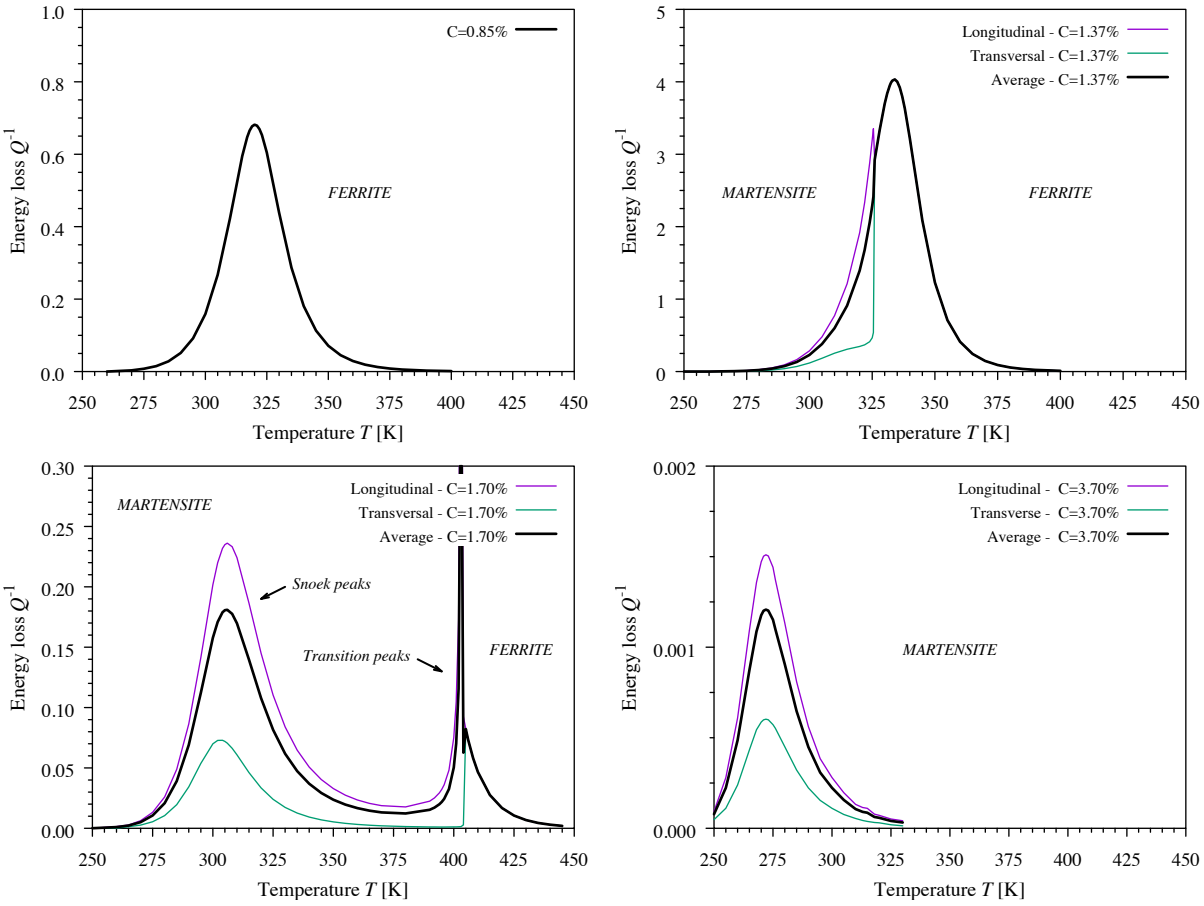

Figure 3: Snoek peaks computed with the thermo-kinetic model for various carbon contents. In the case $C = 1.70$ at% (bottom left) the martensite–ferrite transition peaks are visible at temperature $T = 404$ K. Frequency $f = 1$ Hz.

At $C = 0.85$ at%, the crystal is ferritic over the whole temperature range. Because of the high carbon content in solid solution, the magnitude of the Snoek profile is very high (Fig. 3, top left). The peak position is slightly shifted towards high temperatures ($T_\mathrm{m} = 320$ K) compared to low-carbon ferrite ($T_\mathrm{m} = 310$ K) on account of sluggish carbon diffusivity at high carbon content (see Refs. [30, 36]).

On the other hand, the high-carbon crystal ($C = 3.7$ at%) is martensitic in the whole temperature range. It does exhibit a Snoek peak (Fig. 3, bottom right). Notice that the peak magnitude is reduced compared to ferrite, although the carbon content is higher. The peak position is shifted towards low temperatures. Comparing transversal and longitudinal excitations, the magnitude of the longitudinal peak is 2.5 times that of the transversal peak, but the peak positions appear equal. Contrary to ferrite, where the profiles are almost symmetric, the peaks in martensite are skewed.

The case of medium-carbon martensite ($C = 1.7$ at%) is similar to high-carbon martensite, except that the peak magnitude is much higher and the peak temperature is higher (Fig. 3, bottom left). Notice that the peak temperatures of the transversal and longitudinal profiles differ by 2 degrees. Also, an additional peak appears in the temperature range under investigation. Its maximum is positioned at $T = 404$ K, which identifies with the transition temperature T^+. This peak originates from the martensite $\rightarrow$ ferrite transition, which induces a high energy loss in a narrow temperature range [25]. We checked that the transition peak is athermal: its temperature does not vary with the oscillation frequency, but only with the solute carbon content.

In the case of $C = 1.37$ at%, the transition temperature $T^+ = 327$ K lies in the Snoek profile (Fig. 3, top right). We observe a "giant" Snoek peak ($Q_\mathrm{m}^{-1} = 4.03$). The profile consists of the contribution of martensite when $T < 327$ K followed by the contribution of ferrite when $T > 327$ K. Figure 4 shows the time evolution of the site fractions c_i

during stress cycles applied at 320 K. A stress amplitude of 10 MPa was chosen here to enhance the variations in site fractions. The occupancies of favored (most occupied) and disfavored (least occupied) sites oscillate periodically around their stress-free equilibrium value. Under transversal excitation (Fig. 4, left) c_1 and c_2 vary in mutual phase opposition, which reflects the carbon exchanges between site-1 and site-2. Under longitudinal excitation (Fig. 4, right) the carbon exchanges occur between the favored (c_2) and the disfavored (c_1, c_3) sites.

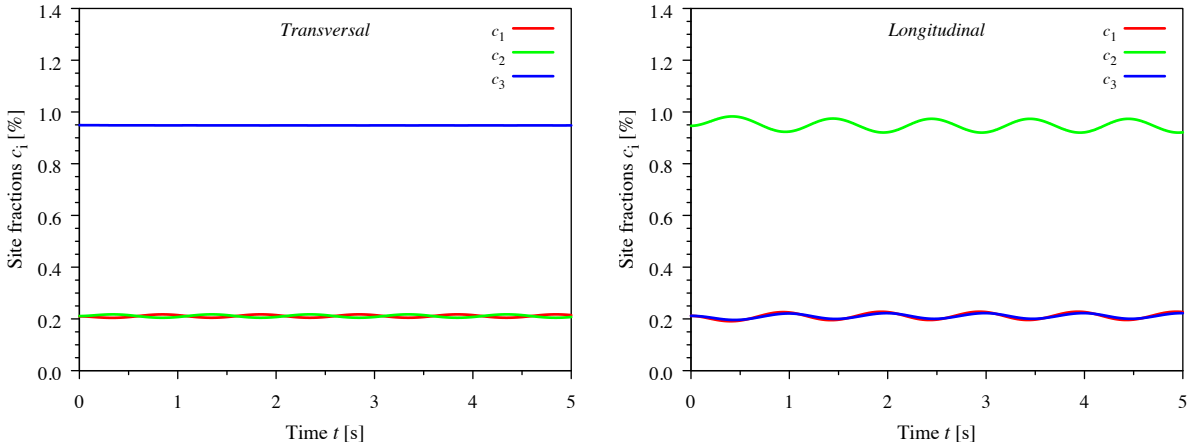

Figure 4: Time evolution of the site fractions during 5 cycles at $f = 1$ Hz calculated with the thermo-kinetic model. Transversal (left) and longitudinal (right) excitations. The occupancies of favored and disfavored sites oscillate periodically around their stress-free equilibrium value, reflecting the carbon exchanges between the various sites. We set $C = 1.37$ at%, $T = 320$ K and $\sigma_0 = 10$ MPa.

3.4. Frequency-dependent Snoek profiles

To study the influence of oscillation frequency on internal friction, we computed a series of Snoek profiles in the frequency range of 10^{-3} to 10^{3} Hz at fixed temperature $T = 300$ K for various carbon contents. In Figure 5, the energy loss and storage compliance are reported as function of frequency in ferrite phase ($C = 0.85$ at%) and martensite phase ($C = 1.70$ at%), close to the ordering transition ($C^{+} = 1.26$ at%). Both energy loss profiles follow a Debye curve, with a relative accuracy better than 0.1%. As a consequence, the frequency dispersion is such that the energy loss Q^{-1} varies as ω^{+1} (resp. ω^{-1}) in the low (resp. high) frequency regime. The fitted relaxation strength and time in the case of martensite are respectively: $\Delta^{\text{trans}} = 0.142$, $\Delta^{\text{longi}} = 0.433$, $\tau^{\text{trans}} = 0.186$ s and $\tau^{\text{longi}} = 0.233$ s. The peak frequency in martensite is located around 1 Hz, i.e. one decade higher than in ferrite (~ 0.1 Hz). This is consistent with a higher peak temperature in ferrite ($T_{\text{m}} = 320$ K) than in martensite ($T_{\text{m}} = 305$ K), see Figure 3.

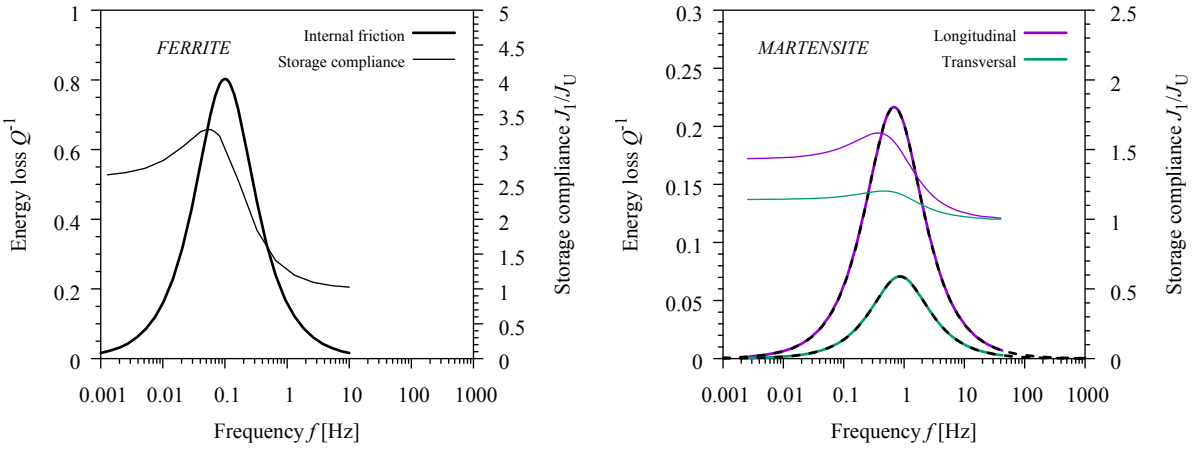

Figure 5: Frequency-dependent energy loss and storage compliance computed with the thermo-kinetic model. Left: highly supersaturated ferrite, $C = 0.85$ at%. Right: martensite, $C = 1.70$ at%. Debye fits are shown in dashed lines. Temperature $T = 300$ K.

The relative storage compliance J_1/J_U reaches the asymptotic value of 1 at high frequencies and the relaxed value J_R/J_U at low frequencies, as expected for a standard anelastic solid [25]. However, when the carbon content is close to the ferrite–martensite transition, the storage compliance shows an unusual peak in the vicinity of the energy loss peak. This is probably due to the high magnitude of both the storage compliance and the energy loss in the ferrite–martensite transition region. Under this circumstance, the usual assumption $\tan(\phi) \ll 1$ no longer holds and deviations

from the standard behavior are expected. Such deviations were not observed in our computations of low-carbon ferrite or high-carbon martensite.

3.5. Effect of solute carbon content

Figure 6 summarizes the effect of carbon content on the Snoek profiles of martensite. Several striking features appear: (i) The peak height varies over several orders of magnitude (10^{-5}–10^{-1}) although the range of composition is relatively narrow (1.7–4.7 at%); (ii) The peak height *decreases* with increasing carbon content; (iii) The peak position is shifted towards lower temperatures and higher frequencies when the carbon content is increased. These features are summarized in Figure 7 where the peak height and temperature are plotted as a function of carbon content. At first sight, the peak height decreases exponentially and the peak temperature decreases linearly with the carbon content. This behavior strongly differs from that of ferrite. Both peak height and peak magnitude in martensite are lower than extrapolation from ferrite would predict.

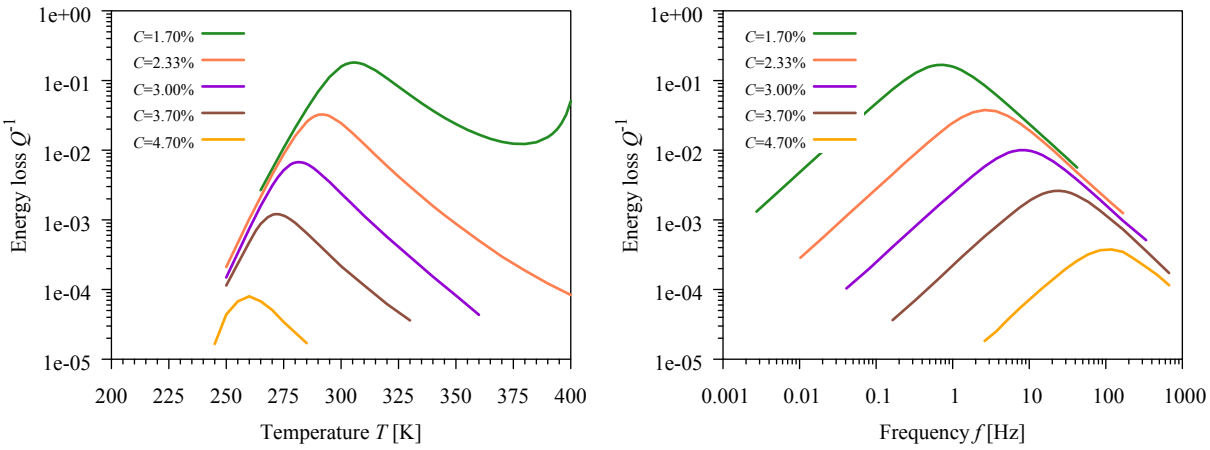

Figure 6: Average Snoek peaks in martensite computed with the thermo-kinetic model. Left: temperature-dependent profiles at frequency $f = 1$ Hz. Right: frequency-dependent profiles at temperature $T = 300$ K. When the carbon content is increased, the peak height decreases while the peak position shifts towards lower temperatures or higher frequencies.

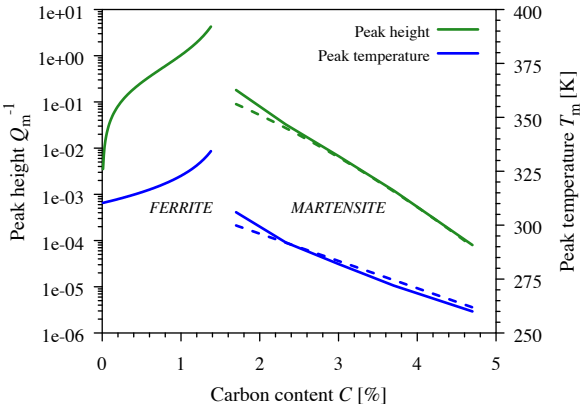

Figure 7: Effect of carbon content on peak height and peak temperature upon cooling in ferrite (from [36]) and upon heating in martensite (this work) computed with the thermo-kinetic model. The single-relaxation approximation is plotted in dashed lines. Frequency $f = 1$ Hz.

4. The linear-response approximation

Our computations assess the existence of a Snoek peak in martensite. However, several features of the calculated energy loss profiles are unexpected, and raise a series of questions. First, the peak height decreases when the carbon content increases, while the opposite in reported in ferrite [2]. Second, the peak temperature is significantly lower in martensite than in ferrite, and it decreases with the carbon content. Third, the peak shape is not symmetric but skewed. Last, one would expect two peaks in martensite, given the two degrees of freedom —associated with the two order parameters— whereas a unique peak is observed. To rationalize these results, we developed a linear-response theory

providing an approximate analytical form of the Snoek profiles. A further simplification termed "single-relaxation approximation" gave analytical expressions of the profile features.

We found an analytical solution to the kinetic equations (Eq. 8) under the linear-response approximation. This approximation consists in linearizing the rate equations with respect to the order parameters ζ, η and the shear stress σ. The approximation is valid in the vicinity of stress-free thermodynamic equilibrium. In their general treatment of the effect of order-disorder transition on relaxation, Nowick and Berry [25] linearized the Gibbs energy function in the vicinity of the *disordered* equilibrium state. This approach was used by the present author to investigate the giant Snoek effect in ferrite [35]. However, as martensite is an ordered alloy, linearization in the vicinity of the *ordered* equilibrium state is needed in the present study. The first step of our resolution was thus to write an analytical expression of the order parameters of martensite at equilibrium.

4.1. Equilibrium order parameters

Starting from the enthalpy function H (Eq. 3) and the regular entropy S in the dilute approximation, the Gibbs energy $G = H - TS$ was written as a function of the external variables C, T and σ, and the internal variables ζ and η [35]. The condition for thermodynamic equilibrium under fixed solute carbon content, temperature and no applied stress is found by minimizing function G with respect to the internal variables ζ and η. Above the order–disorder transition, i.e. at low carbon content or high temperature, the unique solution to the equilibrium equations is $\zeta = \eta = 0$, which corresponds to disordered ferrite. Below the order–disorder transition, there are three couples of degenerate solutions (ζ, η) corresponding to the three ordered orientational variants of martensite. Considering in the first instance the orientational variant-3, whose tetragonal axis lies along crystal direction 3, the solution to these equations is $\zeta = 0$ and $\eta = \eta_0(C, T)$. This solution is presented as a function of T in Figure 8 (left), for a carbon content of $C = 1.7$ at%. The ordering curves of variants-1 and 2 verify $\zeta = -\eta_0(C, T)$ and $\zeta = \eta_0(C, T)$ respectively.

The equilibrium transition temperature in the absence of stress, T_0, is defined by the relationship $k_B T_0 = 1.082\, h_\Sigma C$. T_0 increases linearly with carbon content. The proportionality coefficient contains the strain-energy parameter h_Σ, which characterizes the carbon–strain interaction responsible for ordering. Parameter h_Σ is related to the elastic properties of the octahedral defect:

$$h_\Sigma = \frac{2V_0(\lambda_1 - \lambda_2)^2}{3S'} \tag{9}$$

where $S' = 2(S_{11} - S_{12}) = 0.0167$ GPa^{-1} is the shear compliance. Numerically $h_\Sigma = 1.87$ eV and $T_0 = 235\, C$ (C in at%). On account of hysteresis, the order-disorder transition occurs at a temperature T^+ slightly higher than T_0 when martensite is heated [33]: $T^+ = 238\, C$. At $C = 1.7$ at% corresponding to Figure 8 (left) we have $T_0 = 400$ K and $T^+ = 404$ K.

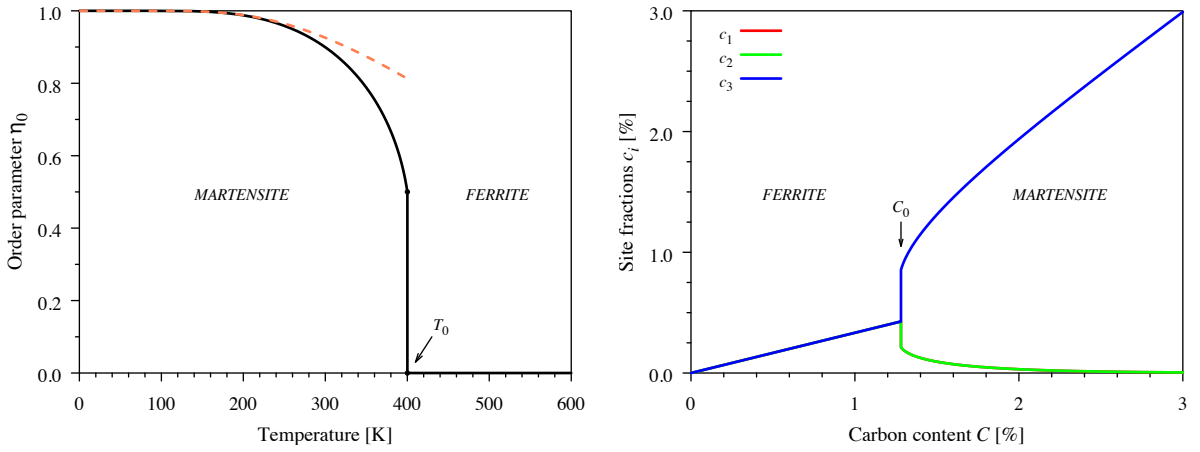

Figure 8: Left: Equilibrium ordering curve as function of temperature for $C = 1.7$ at%. The martensite–ferrite order–disorder transition temperature is $T_0 = 400$ K. The dashed line is the high-carbon low-temperature approximation (Eq. 10). Right: Equilibrium site fractions in variant-3 as function of carbon content at $T = 300$ K. In martensite, fraction c_1 ($= c_2$) decreases towards zero when the total carbon fraction increases.

Far from the order–disorder transition, i.e. in the high-carbon or low-temperature case, the equilibrium order parameter η_0 is close to one. As shown in Figure 8 (left), it is well approximated by the expression

$$\eta_0(C, T) \simeq 1 - 3\exp\left(-\frac{3h_\Sigma C}{k_B T}\right). \tag{10}$$

The activation enthalpy entering this equation is the enthalpy of ordering $H' = 3h_\Sigma C$.

Figure 8 (right) shows the equilibrium site fractions in variant-3 as function of carbon content at temperature $T = 300$ K. The order–disorder transition occurs at carbon fraction $C_0 = 1.28$ at% verifying the relationship $k_B T = 1.082\, h_\Sigma C_0$. In martensite, the Zener order increases with carbon content. Consequently, carbon fractions at the disfavored sites (c_1, c_2) decrease towards zero to the benefit of the favored sites (c_3) when the total carbon fraction increases. From Equation 10 the decrease is nearly an exponential function of C:

$$c_1 = c_2 \simeq C \exp\left(-\frac{3h_\Sigma C}{k_B T}\right). \tag{11}$$

4.2. Characteristic times

By linearizing the rate equations (Eq. 8) and introducing the approximate order parameter (Eq. 10) we obtained the linear differential equations of the order parameters describing the crystal response to either transversal or longitudinal excitation. As will be shown in the next sections, these equations involve two characteristic times of short-range carbon diffusion: (i) τ_{aa} is the characteristic time of carbon exchanges between disfavored sites ($a \leftrightarrow a$); (ii) τ_{ac} is the characteristic time of carbon exchanges between disfavored and favored sites ($a \leftrightarrow c$). These two mechanisms of carbon exchange contribute in parallel to the atom transfer from sites-1 to sites-2 when the shear stress is applied. The characteristic times write in full

$$\begin{cases} \dfrac{1}{\tau_{aa}} = 4\nu_0 \exp\left(-\dfrac{H_0^m + \Delta H_{aa} C}{k_B T}\right) \\ \dfrac{1}{\tau_{ac}} = 2\nu_0 \exp\left(-\dfrac{H_0^m + \Delta H_{ac} C}{k_B T}\right) \end{cases} \tag{12}$$

They are thermally activated and depend on the carbon content via the activation enthalpies, with

$$\begin{cases} \Delta H_{aa} = \Delta\boldsymbol{\lambda}^{12} \cdot \boldsymbol{P}^{O_3} \\ \Delta H_{ac} = \Delta\boldsymbol{\lambda}^{13} \cdot \boldsymbol{P}^{O_3} - \dfrac{3}{2} h_\Sigma \end{cases} \tag{13}$$

where $\Delta\boldsymbol{\lambda}^{ik}$ is the rank-2 tensor

$$\Delta\boldsymbol{\lambda}^{ik} = -\boldsymbol{\lambda}^{T_j} + \frac{\boldsymbol{\lambda}^{O_i} + \boldsymbol{\lambda}^{O_k}}{2}. \tag{14}$$

The two characteristic times differ by their pre-exponential factors and by their activation enthalpies. The terms in the form $\Delta\boldsymbol{\lambda} \cdot \boldsymbol{P}$ in Equations 13 render the effect of the tetragonal distortion of the crystal on the activation barriers. The strain-energy parameter h_Σ in ΔH_{ac} renders the difference in occupancy of sites of type a and c, i.e. the effect of carbon ordering. Incorporating the three migration barriers $H_{a\to a}$, $H_{a\to c}$ and $H_{c\to a}$ between the various sites, we find

$$\begin{cases} \Delta H_{aa} = H_{a\to a} \\ \Delta H_{ac} = \dfrac{1}{2}\left(H_{a\to c} + H_{c\to a}\right) - \dfrac{3}{2} h_\Sigma \end{cases} \tag{15}$$

Thus, the characteristic time τ_{aa} is that of the disfavored → disfavored atomic jumps. On the other hand, the activation enthalpy ΔH_{ac} is related to the average of forward and backward migration barriers between disfavored and favored sites. Taking into account that the energy of sites c is lowered by the quantity $H' = 3h_\Sigma C$ in the high-carbon approximation, we have $H_{c\to a} = H_{a\to c} + 3h_\Sigma C$. The term $\frac{3}{2}h_\Sigma$ in Equation 15 cancels out, such that finally $\Delta H_{ac} = H_{a\to c}$. Thus, the characteristic time τ_{ac} identifies with the disfavored → favored atomic jumps. As will be shown in a next section, the disfavored ↔ disfavored exchanges are much slower than the disfavored ↔ favored ones, such that $\tau_{aa} \gg \tau_{ac}$.

A singularity of martensite as compared to ferrite resides in the relaxation of *two* order parameters in martensite rather than a unique parameter in ferrite [35]. The consequences of this are examined in the following sections.

4.3. Case of transversal excitation

To study the effect of a transversal applied stress, we considered variant-3, whose tetragonality axis is parallel to the shear axis (see Figure 1, right). At stress-free equilibrium, disfavored sites-1 and 2 are equally occupied. A positive shear stress exerts tension along axis-2 and compression along axis-1, thus creating a bias in chemical potential to the advantage of sites-2, at the expense of sites-1. As a consequence, sites-1 deplete to the benefit of sites-2. The opposite occurs when the stress is reversed (see Fig. 4, left). This stress-induced atom transfer is the origin of Snoek relaxation under transversal excitation. It is reflected by the time evolution of order parameter ζ.

The stress-induced deviations from stress-free equilibrium order are defined as $\Delta\zeta = \zeta(\sigma)$ and $\Delta\eta = \eta(\sigma) - \eta_0$. The relaxed state, corresponding to the conditions $\dot{\zeta} = \dot{\eta} = 0$, was determined analytically from the linearized rate equations. It appears that the relaxed value of $\Delta\eta$ is not affected by the applied stress. Then, to the first order, η

remains equal to its stress-free equilibrium value during an internal friction measurement or a relaxation test: the relaxed value $\Delta\eta_R = 0$. The applied stress only affects the order parameter ζ. Its relaxed value is expressed as

$$\zeta_{\mathrm{R}} = 2\frac{V_0(\lambda_1 - \lambda_2)}{k_{\mathrm{B}}T}\exp\left(-\frac{3h_\Sigma C}{k_{\mathrm{B}}T}\right)\sigma, \tag{16}$$

valid for $C \gg C_0$. The exponential factor in ζ_{R} originates from the C and T dependence of the equilibrium order parameters of tetragonal martensite (Eq. 10). This expression of ζ_{R} in martensite differs by an exponential factor from the classical expression for low-carbon ferrite, valid when $C \ll C_0$:

$$\zeta_{\mathrm{R}}^{\mathrm{ferr}} = \frac{2}{3}\frac{V_0(\lambda_1 - \lambda_2)}{k_{\mathrm{B}}T}\sigma. \tag{17}$$

Whereas the relaxed value is composition independent in ferrite, it has the striking feature of *decreasing* with the solute carbon content in martensite. Notice that the ratio $\zeta_{\mathrm{R}}/\zeta_{\mathrm{R}}^{\mathrm{ferr}} = 3\exp(-3h_\Sigma C/k_{\mathrm{B}}T)$ decreases exponentially with C. The reason is as follows: in ferrite, all solute carbon atoms can participate to the anelastic response. Conversely, in variant-3 martensite most carbon atoms occupy sites-3, such that the number of carbon atoms located in sites-1 and 2 is reduced by a factor of $3\exp(-3h_\Sigma C/k_{\mathrm{B}}T)$ compared to ferrite (see Eq. 11). Under transversal excitation, only this small proportion of atoms participates to the anelastic response. The proportion decreases with the carbon content on account of the increase in Zener ordering (see Section 4.1).

Following an equivalent approach to Nowick and Berry [25], we now look for the relaxation of the strain when a prior constant stress σ is suppressed at time $t = 0$. From the time dependence of the strain, the relaxation time τ and the relaxation strength Δ can be extracted. The linearized rate equations are written, in case of transversal excitation,

$$\begin{cases} \dfrac{\mathrm{d}\zeta}{\mathrm{d}t} = -\left(\dfrac{1}{\tau_{\mathrm{ac}}} + \dfrac{1}{\tau_{\mathrm{aa}}}\right)(\zeta - \zeta_R) \\ \dfrac{\mathrm{d}\eta}{\mathrm{d}t} = 0 \end{cases} \tag{18}$$

From Equation 1, the shear strain as reference to stress-free martensite is

$$\varepsilon = S'\sigma + (\lambda_1 - \lambda_2)C\zeta. \tag{19}$$

The first term in the right-hand side is the elastic response ε_{U} while the second term is the anelastic response $\varepsilon_{\mathrm{an}}$. Solving Eq. 18 and using Eq. 19, we find a typical time evolution of the anelastic strain:

$$\frac{\varepsilon_{\mathrm{an}}(t)}{\varepsilon_{\mathrm{U}}} = \Delta^{\mathrm{trans}}\exp\left(-\frac{t}{\tau^{\mathrm{trans}}}\right). \tag{20}$$

The relaxation time τ^{trans} entering Equation 20 combines both characteristic times τ_{ac} and τ_{aa}:

$$\frac{1}{\tau^{\mathrm{trans}}} = \frac{1}{\tau_{\mathrm{ac}}} + \frac{1}{\tau_{\mathrm{aa}}}. \tag{21}$$

Interpretation of this result is as follows: when a positive shear stress σ is applied, the site occupancy is slightly biased is favor of type-2 sites. When the stress is suppressed, relaxation occurs by two mechanisms in parallel: (i) direct exchange $2 \to 1$ between disfavored sites, associated to the characteristic time τ_{aa}; and (ii) indirect exchange along the path $2 \to 3 \to 1$ via favored type-3 sites, associated to the characteristic time τ_{ac}. Since $\tau_{\mathrm{aa}} \gg \tau_{\mathrm{ac}}$, we have $\tau^{\mathrm{trans}} \simeq \tau_{\mathrm{ac}}$, i.e. relaxation is provided mostly by *indirect* exchange. This finding is coherent with the anisotropy of diffusivity evidenced in martensite [30]: diffusion is fast in the $x - y$ plane thanks to $a \to c \to a$ chains, and slow along the z direction by $a \leftrightarrow a$ exchanges.

The relaxation strength entering Equation 20 is expressed as

$$\Delta^{\mathrm{trans}} = \left(\frac{3h_\Sigma C}{k_{\mathrm{B}}T}\right)\exp\left(-\frac{3h_\Sigma C}{k_{\mathrm{B}}T}\right). \tag{22}$$

Compared to the relaxation strength in ferrite $\Delta^{\mathrm{ferr}} = h_\Sigma C/k_{\mathrm{B}}T$ [35], the relaxation strength in martensite is reduced by the factor $3\exp(-3h_\Sigma C/k_{\mathrm{B}}T)$, which expresses depletion of the disfavored sites to the benefit of the favored ones. Furthermore, conversely to ferrite, the higher the solute carbon content of martensite, the lower is the magnitude of the relaxation strength.

From the above calculation, we conclude that during an internal friction measurement producing a transversal excitation at angular frequency ω, the energy loss will follow a Debye curve associated to the relaxation strength Δ^{trans} and the relaxation time τ^{trans}:

$$Q^{-1}_{\mathrm{trans}} = \Delta^{\mathrm{trans}}\frac{\omega\tau^{\mathrm{trans}}}{1 + (\omega\tau^{\mathrm{trans}})^2} \tag{23}$$

This formula and Equations 21–22 constitute the linear-response approximation of the energy loss of martensite under transversal excitation.

4.4. Case of longitudinal excitation

In the case of longitudinal excitation, the tetragonality axis of the crystal is oriented along direction 2 (see Fig. 1, right). Favored sites-2 are largely more occupied than disfavored sites-1 and 3. However, at stress-free equilibrium, favored and disfavored sites share the same value of the chemical potential. A positive shear stress creates a bias in chemical potential to the advantage of sites-2, at the expense of sites-1 and 3. As a result, a small proportion of carbon atoms leave the disfavored sites to the benefit of the favored ones. An opposite flux sets up if the stress is reversed, i.e. the favored sites deplete to the benefit of the disfavored ones (see Fig. 4, right). This stress-induced atom transfer is the origin of Snoek relaxation under longitudinal excitation. It is reflected by the time evolution of both order parameters ζ and η.

At stress-free equilibrium the order parameters are $\zeta = \eta_0(C,T)$ and $\eta = -\frac{1}{2}\eta_0(C,T)$. Introducing the deviations from stress-free equilibrium as $\Delta\zeta = \zeta(\sigma) - \eta_0$ and $\Delta\eta = \eta(\sigma) + \frac{1}{2}\eta_0$, and using the approximation of Equation 10, we find the relaxed values

$$\begin{cases} \Delta\zeta_{\mathrm{R}} = 5\dfrac{V_0(\lambda_1-\lambda_2)}{k_{\mathrm{B}}T}\exp\left(-\dfrac{3h_\Sigma C}{k_{\mathrm{B}}T}\right)\sigma \\ \Delta\eta_{\mathrm{R}} = -\dfrac{3}{2}\dfrac{V_0(\lambda_1-\lambda_2)}{k_{\mathrm{B}}T}\exp\left(-\dfrac{3h_\Sigma C}{k_{\mathrm{B}}T}\right)\sigma \end{cases} \tag{24}$$

Contrary to the transversal case, the rate equations of $\Delta\zeta$ and $\Delta\eta$ are now coupled:

$$\begin{cases} \dfrac{\mathrm{d}\Delta\zeta}{\mathrm{d}t} = -\left(\dfrac{1}{\tau_{\mathrm{ac}}} + \dfrac{1}{4\tau_{\mathrm{aa}}}\right)(\Delta\zeta - \Delta\zeta_{\mathrm{R}}) - \dfrac{1}{2\tau_{\mathrm{aa}}}(\Delta\eta - \Delta\eta_{\mathrm{R}}) \\ \dfrac{\mathrm{d}\Delta\eta}{\mathrm{d}t} = -\dfrac{3}{8\tau_{\mathrm{aa}}}(\Delta\zeta - \Delta\zeta_{\mathrm{R}}) - \left(\dfrac{1}{\tau_{\mathrm{ac}}} + \dfrac{3}{4\tau_{\mathrm{aa}}}\right)(\Delta\eta - \Delta\eta_{\mathrm{R}}) \end{cases} \tag{25}$$

This system of linear differential equations admits two eigen modes of relaxation, labeled parallel ($\|$) and perpendicular ($\perp$). The associated eigen values are defined by

$$\begin{cases} \dfrac{1}{\tau_{\|}} = \dfrac{1}{\tau_{\mathrm{ac}}} \\ \dfrac{1}{\tau_{\perp}} = \dfrac{1}{\tau_{\mathrm{ac}}} + \dfrac{1}{\tau_{\mathrm{aa}}} \end{cases} \tag{26}$$

$\tau_{\|}$ is the relaxation time of variable $\eta' = \left(c_2 - \frac{1}{2}(c_1+c_3)\right)/C$, which quantifies Zener ordering along direction-2. $\tau_{\perp}$ is the relaxation time of variable $\zeta' = (c_3 - c_1)/C$, which quantifies the degree of orthorhombicity, or "beyond Zener" ordering [31]. As discussed above, $\tau_{\mathrm{aa}} \gg \tau_{\mathrm{ac}}$, such that the relaxation times $\tau_{\|}$ and $\tau_{\perp}$ are very close to one another. Notice that $\tau_{\perp}$ is identical to the relaxation time under transversal excitation τ^{trans} (Eq. 21). The solution to Equations 25 together with the strain Equation 19, yield the time evolution of the anelastic strain during relaxation:

$$\frac{\varepsilon^{\mathrm{an}}(t)}{\varepsilon_{\mathrm{U}}} = \Delta_{\|}\exp\left(-\frac{t}{\tau_{\|}}\right) + \Delta_{\perp}\exp\left(-\frac{t}{\tau_{\perp}}\right), \tag{27}$$

with the relaxation strengths of the $\|$ and $\perp$ modes:

$$\begin{cases} \Delta_{\|} = \dfrac{9}{4}\left(\dfrac{3h_\Sigma C}{k_{\mathrm{B}}T}\right)\exp\left(-\dfrac{3h_\Sigma C}{k_{\mathrm{B}}T}\right) \\ \Delta_{\perp} = \dfrac{1}{4}\left(\dfrac{3h_\Sigma C}{k_{\mathrm{B}}T}\right)\exp\left(-\dfrac{3h_\Sigma C}{k_{\mathrm{B}}T}\right) \end{cases} \tag{28}$$

Relaxation strength of the parallel mode ($\Delta_{\|}$) happens to be 9 times more intense than that of the perpendicular mode ($\Delta_{\perp}$).

From Equation 27 we conclude that the energy loss under longitudinal excitation is the sum of two Debye curves corresponding to the parallel and the perpendicular modes of relaxation, respectively:

$$Q^{-1}_{\mathrm{longi}} = \Delta_{\|}\frac{\omega\tau_{\|}}{1+(\omega\tau_{\|})^2} + \Delta_{\perp}\frac{\omega\tau_{\perp}}{1+(\omega\tau_{\perp})^2} \tag{29}$$

4.5. Comparison with the thermo-kinetic model

To test our analytical approach, we compared numerically the linear-response approximation (Eqs. 23 and 29) to the thermo-kinetic model. Figure 9 presents the energy losses in case of transversal (left) and longitudinal (right) excitations when C is set to 3 at%. In the longitudinal case, contributions of the parallel and perpendicular modes

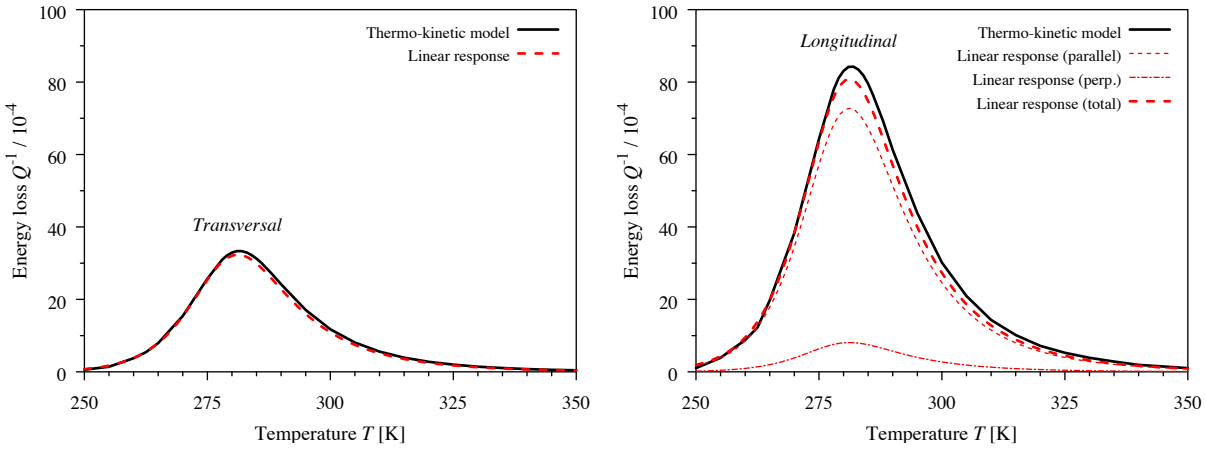

Figure 9: Comparison between the thermo-kinetic model and the linear-response approximation. Snoek peaks computed under transversal (left) and longitudinal (right) excitations. Carbon content $C = 3$ at%, frequency $f = 1$ Hz.

are presented. The agreement between both approaches is within 5% at the peak maximum, which validates the linear-response approximation.

From the linear-response approximation (Eqs. 12, 13 and 14) the activation enthalpies of the characteristic times write numerically (in eV): $H_{aa} = 0.872 + 378\,C$ and $H_{ac} = 0.872 - 379\,C$ (C in at%). For the 3 at% carbon alloy under consideration, this gives $H_{aa} = 0.985$ eV and $H_{ac} = 0.758$ eV. As a result, the characteristic time of the $a \leftrightarrow a$ exchanges is much larger than that of the $a \leftrightarrow c$ exchanges. For instance at 300 K, $\tau_{aa} = 60.2$ s while $\tau_{ac} = 0.0184$ s. As a consequence the relaxation times of all modes are nearly equal: $\tau_{\parallel} \simeq \tau_{\perp} \simeq \tau^{\text{trans}} = 0.0184$ s. They are much reduced compared to ferrite ($\tau^{\text{ferr}} = 0.499$ s [35]), which explains the downward shift of the peak temperature in martensite.

4.6. The single-relaxation approximation

The linear-response approximation provides analytic expressions of the internal friction temperature profiles. From these expressions, analytical formulae of the peak temperature T_m and the peak height Q_m^{-1} could be approximated.

We recall that the characteristic time τ_{aa} is very long compared to τ_{ac}. In the single-relaxation approximation, we neglect τ_{aa}^{-1} as regards to τ_{ac}^{-1} in the expressions of the relaxation times (Eqs. 21 and 26). Under this approximation, all relaxation times are equal, and will be denoted τ. τ has the universal form $\tau = \tau_0 \exp(H/k_B T)$, with a constant pre-exponential factor $\tau_0 = (2\nu_0)^{-1}$ and a carbon-dependent activation energy $H = H_0^m + \Delta H_{ac} C$. Because all modes share the same relaxation time, they have the same temperature dependence, but their amplitudes differ. From Equations 22 and 28 of the relaxation strengths, the longitudinal modes sum to $\Delta^{\text{longi}} = \frac{5}{2}\Delta^{\text{trans}}$. Then, the average relaxation strength amounts to $\Delta = 2\Delta^{\text{trans}}$.

It is noteworthy that, contrary to ferrite, the relaxation strength in martensite is highly temperature dependent via the enthalpy of ordering $H' = 3h_\Sigma C$. In full, the average energy loss in the single-relaxation approximation writes as a function of temperature

$$Q^{-1}(T) = 2\left(\frac{H'}{k_B T}\right)\exp\left(-\frac{H'}{k_B T}\right)\frac{\omega\tau_0 \exp\left(\frac{H}{k_B T}\right)}{1 + \left(\omega\tau_0 \exp\left(\frac{H}{k_B T}\right)\right)^2} \tag{30}$$

The frequency dependence of Q^{-1} has the form of a Debye curve with a temperature-dependent relaxation strength $\Delta(T)$. If the relaxation strength was temperature independent, the temperature profile would have the form of an inverse cosh function of $1/T$, and the energy loss would peak at temperature $k_B T_m^0 = -H/\ln(\omega\tau_0)$. In view of Equation 30, this is not the case here. Performing a first-order development of $Q^{-1}(T)$ around T_m^0 gives an approximate expression of the actual peak temperature T_m:

$$k_B T_m = -\frac{H}{\ln(\omega\tau_0)} + \frac{2H'}{(\ln(\omega\tau_0))^2} \tag{31}$$

We see that the peak temperature is higher than T_m^0 on account of carbon ordering ($H' = 562\,C > 0$). Numerically, the difference is of the order of a few degrees. T_m decreases linearly with the carbon content mostly by the composition dependence of the relaxation time ($H = 0.872 - 379\,C$). Thus, the enhancement of the carbon exchanges between disfavored and favored sites induced by the Zener ordering is the origin of the downward shift of the peak temperature when the carbon content is increased.

The zeroth-order approximation of the peak height is $\Delta(T_m^0)/2$, i.e.

$$Q_m^{-1} = -\frac{H'}{H}\ln(\omega\tau_0)\exp\left(\frac{H'}{H}\ln(\omega\tau_0)\right). \tag{32}$$

Q_m^{-1} is composition-dependent via both the thermodynamic effect (H') and the kinetic effect (H) of solute carbon. Since function $\frac{H'}{H}\ln(\omega\tau_0)$ in Equation 32 is negative and decreases with C, the peak height is a decreasing function of the carbon content. The peak height is also frequency-dependent: it increases with the oscillation frequency.

Formulae 31 and 32 provide an excellent estimate of the peak characteristics of martensite in the composition range of 2 to 5 at% (Figure 7). A slight discrepancy is observed at lower carbon content, where the approximation $C \gg C_0$ is no longer valid. Numerically, at the oscillation frequency of 1 Hz, the peak temperature equals 296 K at 2 at%C and decreases by 12.7 degrees per atomic percent of carbon: $T_m = 321 - 12.7\,C$ (at%). The peak height roughly loses one decade per atomic percent of carbon.

5. Discussion

5.1. Martensite vs ferrite

Our theoretical investigation shows that bct-martensite does present Snoek relaxation via short-range diffusion of solute carbon atoms. This relaxation differs in many ways from Snoek relaxation in ferrite:

1. Due to the tetragonal symmetry of martensite, the three {100} planes are not all equivalent, and the relaxation kinetics depends on whether the applied shear stress is longitudinal or transversal with reference to the tetragonality axis;
2. Short-range diffusion of carbon is anisotropic and involves two characteristic times, instead of a single one in ferrite;
3. Carbon content has an effect on the relaxation kinetics: indirect exchanges in the perpendicular plane are accelerated when the carbon content is increased;
4. Carbon ordering in martensite has two degrees of freedom —associated with two order parameters—, which generates two modes of relaxation (parallel and perpendicular).

As a consequence, the temperature-dependent Snoek profiles show original features, opposite to what is observed in ferrite:

1. The peak height decreases when the carbon content increases;
2. The peak temperature decreases when the carbon content increases;
3. The peak shape is skewed.

Our analysis shows that point (1) is due to the depletion of the disfavored interstitial sites when the carbon content is increased. Point (2) is due to accelerated carbon jumps in the plane perpendicular to the tetragonal axis when the carbon content increases. Point (3) is due to the temperature-dependent depletion of the disfavored sites.

5.2. On the occurrence of Snoek peak in martensite

It has been alleged in the literature that Snoek relaxation in tetragonal martensite is impossible. Two arguments were put forward by some authors:

1. Ward and Capus [15], cited later by Tkalcec et al. [10] wrote: "In fact, the tetragonality of the martensite precludes the presence of equivalent octahedral sites in the lattice cell that is needed for the point defects to give rise to anelastic relaxation." This symmetry argument is rebuttable: Indeed, favored site-1 and 2 of variant-3 are equivalent sites. Hence, the bias created by a transversal excitation leads to relaxation by carbon exchanges between these sites.
2. Johnson [26], cited by Klems et al. [22] assessed that "The mechanism for such an effect in martensite involves the application of a sufficiently great applied stress to make an O_a site energetically more favorable than an O_c site". The argument has been taken up by Iwasaki et al. [27]. Our answer is two-fold. First, in order to get a relaxation response, there is no need for a massive change of carbon occupancy from previously favored sites towards newly energetically favored sites: actually, a minute transfer of carbon atoms is sufficient to provide a measurable signal. Hence, the internal friction signal is obtained thanks to small periodic variations of the tetragonality, without a change of the variant orientation (see Fig. 4). Second, the driving force for relaxation is not the bias in energy, but the bias in *chemical potential* between sites (either disfavored/disfavored or disfavored/favored), which induces a carbon flux according to Onsager law [42, 43]. Experiments on ferrite have shown that a stress magnitude as small as 1 MPa is sufficient to produce a measurable energy loss. Our calculations show that the same applies to martensite.

One may argue that "trapping" of carbon atoms in favored sites prevents their jumping out towards disfavored sites. Indeed, it was evidenced theoretically that the migration enthalpy out of favored sites is increased by the carbon content [28, 30]. However, our analysis shows that relaxation is not controlled by this single $c \rightarrow a$ jump, but is dominated by the fast indirect $a \rightarrow c \rightarrow a$ exchange, of characteristic time τ_{ac}. The resulting relaxation kinetics has the unexpected property of being *accelerated* by an increase in carbon content.

5.3. Comparison with experiment

According to our results, the Snoek peak of bct-martensite is expected in the temperature range of 250–310 K for an oscillation frequency of 1 Hz, depending on solute carbon content. Few authors have explored this temperature domain and investigated the effect of carbon content on internal friction. Ward and Capus [15] report internal friction of as-quenched plain carbon martensite (0.015–0.58 wt%C) measured at temperatures greater than 290 K [12–14]: a Snoek-type profile is partly visible in the temperature range of 290–350 K. Prioul [4] interpreted a Snoek-like peak 'B' at ~ 255K in Fe-27Ni-0.18C and Fe-19Ni-0.51C alloyed martensite as originating from the dislocation–solute interaction (Schoeck-Seeger theory [44]). More recently, Liu et al. [5–7] identified the 'M3' peak in Fe-Ni-C virgin martensite (25–28%Ni, 0.2–2.73 wt%C) at 255 K for 0.25 Hz. This peak was attributed to the interactions between carbon atoms and dislocations. Ullakko et al. [8] also attributed their 'A4' peak around 250 K at 0.5 Hz in Fe-Ni-C martensite (20–30%Ni) to dislocation–solute interaction, while Hoyos et al. [11] interpreted their 'P3' peak at 260 K 3 Hz (0.626 and 0.71 wt%C) as the generation of kink pairs in the edge dislocations.

Among the above-cited results, the internal friction profiles of Ward and Capus [15] and of Liu et al. [5] have the original feature of a decreasing peak height when the carbon content is increased. Moreover, the activation energy retrieved by Liu et al. [7] decreases when increasing the carbon content. These features are coherent with our theory and suggest that the peaks identified by these authors is the Snoek peak of martensite. Beyond this qualitative agreement, a quantitative comparison between experiment and theory is hardly reliably because (i) the real carbon content of the solid solution remains unknown on account of carbon segregation and precipitation during auto-tempering and room-temperature aging; (ii) the influence of nickel is not yet included in our model; and (iii) the presence of high internal stress in martensite (coherency stress and dislocation stress field) alter the Snoek response.

5.4. Suggested experimental set up

A clear evidence of the Snoek peak in martensite is still lacking. In view of our results and the difficulties related to temperature-dependent internal friction experiments, we suggest the following experimental set up as an attempt to evidence the Snoek peak. To maximize the carbon content in solid solution, austenite should be quenched from a temperature as low as possible to reduce the effect of auto-tempering, down to a cryogenic temperature, and kept in liquid nitrogen to avoid aging. The energy loss would preferentially be measured in a low temperature range (around 200 K) such as to avoid tempering during the experiment: either by varying the temperature with a very low oscillation frequency, or by varying the oscillation frequency at a low temperature. To test the effect of carbon content on the profile characteristics, samples with various nominal carbon contents, higher than 0.2 wt% should be tested. The amount of solute carbon in martensite would be measured systematically on the quenched specimens (for instance by atom probe tomography), together with the tetragonality ratio.

6. Conclusion

We investigated theoretically the Snoek relaxation in defect-free bct-martensite crystals. The alloy thermodynamics and the carbon migration kinetics were based on a mean-field approximation of the carbon–strain interaction. According to our Monte Carlo simulations, thermo-kinetic modeling and analytical analysis, Snoek relaxation does occur in bct-martensite. The Snoek peak of temperature-dependent energy loss profiles shows original features, related to the peculiarities of Zener-ordered bct-martensite:

1. The peak height decreases when the carbon content is increased, opposite to what occurs in ferrite;
2. The peak temperature depends on the carbon content, and decreases when the carbon content increases.

With an oscillation frequency of 1 Hz, we expect a Snoek peak in the range of temperature of 260 to 305 K for carbon contents of 1.7 to 4.7 at% (0.38–1.05 wt%). This suggests that some peaks reported in the literature may be re-interpreted as genuine Snoek peaks. Further work is planned to investigate the influence of dislocation strain fields on the Snoek-like response of martensite.

Declaration of Competing Interest

The authors declare that they have no known competing financial interests or personal relationships that could have appeared to influence the work reported in this paper.

Acknowledgments

This work was supported by the Agence Nationale de la Recherche, France (contract C-TRAM ANR- 18-CE92-0021).

References

[1] E. Lenz, W. Dahl, Ermittlung von gelöstem Kohlenstoff und Stickstoff mit einem Torsionspendel für streifenförmige Proben, Arch. für das Eisenhüttenwes. 45 (8) (1974) 541–544.
[2] M. Blanter, I. Golovin, H. Neuhauser, H.-R. Sinning, Internal Friction in Metallic Materials, 1st Edition, Springer-Verlag, Berlin Heidelberg, 2007.
[3] D. H. Sulistiyo, L. Cho, E. J. Seo, B. C. De Cooman, Internal friction analysis of lath martensite in press hardened steel, Mater. Sci. Technol. 33 (7) (2017) 879–892.
[4] C. Prioul, Snoek like relaxation in Fe-Ni-C virgin martensite, J. Phys. Colloq. 46 (C10) (1985) 665–668.
[5] Y. Liu, Internal friction associated with dislocation relaxations in virgin martensite-I. Experiments, Acta Metall. Mater. 41 (11) (1993) 3277–3287.
[6] Y. Liu, Effects of martensite morphology on the aging behaviour of virgin martensite, Acta Metall. Mater. 41 (5) (1993) 1587–1593.
[7] Y. Liu, Internal friction associated with dislocation relaxations in virgin martensite-II. Interpretation, Acta Metall. Mater. 42 (3) (1994) 621–630.
[8] K. Ullakko, V. G. Gavriljuk, V. M. Nadutov, Aging of freshly formed Fe- based martensites at low temperatures, Metall. Mater. Trans. A 25 (5) (1994) 889–909.
[9] R. Bagramov, D. Mari, W. Benoit, Internal friction in a martensitic high-carbon steel, Phil. Mag. A 81 (12) (2001) 2797–2808.
[10] I. Tkalcec, D. Mari, W. Benoit, Correlation between internal friction background and the concentration of carbon in solid solution in a martensitic steel, Mater. Sci. Eng. A 442 (1-2 SPEC. ISS.) (2006) 471–475.
[11] J. J. Hoyos, A. A. Ghilarducci, H. R. Salva, C. A. Chaves, J. M. Vélez, Internal friction in martensitic carbon steels, Mater. Sci. Eng. A 521-522 (2009) 347–350.
[12] I. Chernikova, Study of the tempering of quenched steel by the internal friction method, Phys. Met. Metallogr. 5 (1957) 81–84.
[13] V. E. Scheil, E. Wachtel, G. Gurbaxani, Die mechanische Dämpfung von Stählen nach, dem Härten und Anlassen, Arch. für das Eisenhüttenwes. 30 (1959) 497–501.
[14] T. Ichiyama, M. Kawasaki, K. Tkashina, Internal friction in martensite and tempered martensite, J. Japan Inst. Met. 24 (1960) 456–460.
[15] R. Ward, J. M. Capus, Internal friction effects in martensite, J. Iron Steel Inst. 201 (December) (1963) 1038–1043.
[16] G. Speich, Tempering of low-carbon martensite, Trans. Met. Soc. AIME 245 (1969) 2553–2564.
[17] R. Martin, D. Mari, R. Schaller, Influence of the carbon content on dislocation relaxation in martensitic steels, Mater. Sci. Eng. A 521-522 (2009) 117–120.
[18] X. Lu, M. Jin, H. Zhao, W. Li, X. Jin, Origin of low-temperature shoulder internal friction peak of Snoek-Köster peak in a medium carbon high alloyed steel, Solid State Commun. 195 (2014) 31–34.
[19] J. Hoyos, A. Ghilarducci, D. Mari, Evaluation of dislocation density and interstitial carbon content in quenched and tempered steel by internal friction, Mater. Sci. Eng. A 640 (2015) 460–464.
[20] J. Hoyos, D. Mari, Comment on "Origin of low-temperature shoulder internal friction peak of Snoek–Köster peak in a medium carbon high alloyed steel" by Lu et al. [Solid State Communications 195 (2014) 31], Solid State Commun. 226 (2016) 51–53.
[21] T.-S. Kê, Y.-L. Ma, Internal friction peak associated with the stress-induced diffusion of carbon in low-carbon alloy martensite, Sci. Sin. 6 (1) (1957) 81–90.
[22] G. J. Klems, R. E. Miner, F. A. Hultgren, R. Gibala, Internal friction in ferrous martensites, Metall. Trans. A 7 (5) (1976) 839–849.
[23] V. Gavriljuk, V. Duz, K. Ullakko, Internal friction of tempered ferrous martensites, Scr. Metall. Mater. 26 (4) (1992) 667–672.
[24] S. M. Bugaychuk, Y. B. Park, Electronic irradiation modification in parent Fe-Ni-C austenite and Snoek-like effects in induced alpha-martensite, Mater. Sci. Eng. A 370 (1-2) (2004) 127–130.
[25] A. S. Nowick, B. Berry, Anelastic relaxation in crystalline solids, Materials science series [v. 1], Academic Press, New York, 1972.
[26] R. Johnson, Calculation of the energy and migration characteristics of carbon in martensite, Acta Metall. 13 (12) (1965) 1259–1262.
[27] Y. Iwasaki, K. Hashiguchi, Snoek and Snoek-Köster-like Relaxations in Low Carbon Steel with Ferrite-Martensite Dual Phase Structure, Trans. Japan Inst. Met. 23 (5) (1982) 243–249.
[28] B. Lawrence, C. W. Sinclair, M. Perez, Carbon diffusion in supersaturated ferrite : A comparison of mean-field and atomistic predictions, Model. Simul. Mater. Sci. Eng. 22 (2014) 1–17.
[29] D. R. Trinkle, Diffusivity and derivatives for interstitial solutes: activation energy, volume, and elastodiffusion tensors, Philos. Mag. 96 (26) (2016) 2714–2735.
[30] P. Maugis, S. Chentouf, D. Connétable, Stress-controlled carbon diffusion channeling in bct-iron: A mean-field theory, J. Alloys Compd. 769 (2018) 1121–1131.
[31] P. Maugis, A Temperature–Stress Phase Diagram of Carbon-Supersaturated bcc-Iron, Exhibiting "Beyond-Zener" Ordering, J. Phase Equilibria Diffus. 41 (2020) 269–275.
[32] P. Maugis, D. Connétable, P. Eyméoud, Stability of Zener order in martensite: an atomistic evidence, Scr. Mater. 194 (2021) 113632.
[33] P. Maugis, F. Danoix, H. Zapolsky, S. Cazottes, M. Gouné, Temperature hysteresis of the order-disorder transition in carbon-supersaturated α-Fe, Phys. Rev. B 96 (21) (2017) 214104.
[34] P. Maugis, Nonlinear elastic behavior of iron-carbon alloys at the nanoscale, Comput. Mater. Sci. 159 (2019) 460–469.
[35] P. Maugis, Giant Snoek peak in ferrite due to carbon-carbon strain interactions, Materialia 12 (8) (2020) 100805.
[36] P. Maugis, Thermo-kinetic modelling of the giant Snoek effect in carbon-supersaturated iron, J. Alloys Compd. 877 (2021) 160236.
[37] C. Zener, Theory of strain interaction of solute atoms, Phys. Rev. 74 (6) (1948) 639–647.
[38] P. Maugis, Ferrite, martensite and supercritical iron: A coherent elastochemical theory of stress-induced carbon ordering in steel, Acta Mater. 158 (2018) 454–465.
[39] J. da Silva, R. B. McLellan, Diffusion of carbon and nitrogen in B.C.C. iron, Mater. Sci. Eng. 26 (1) (1976) 83–87.
[40] M. Weller, The Snoek relaxation in bcc metals-From steel wire to meteorites, Mater. Sci. Eng. A 442 (1-2 SPEC. ISS.) (2006) 21–30.
[41] L. Huang, P. Maugis, Effect of substitutional Ni atoms on the Snoek relaxation in ferrite and martensite Fe-C alloys : An atomisitic investigation, Comput. Mater. Sci. 203 (2022) 111083.
[42] L. Onsager, Reciprocal relations in irreversible processes. I., Phys. Rev. 37 (1931) 405–426.
[43] L. Onsager, Reciprocal relations in irreversible processes. II., Phys. Rev. 38 (1931) 2265–2279.
[44] G. Schoeck, A. Seeger, The flow stress of iron and its dependence on impurities, Acta Metall. 7 (7) (1959) 469–477.